PAPER

Check for updates

Molecular geometry and the photophysics of thermally activated delayed fluorescence: the strange case of DMAC-py-TRZ†‡

Ettore Crovini,§[a] Rama Dhali,§[b] Dianming Sun, [ID] *[a] Tomas Matulaitis, [ID] [a]
Thomas Comerford, [ID] [a] Alexandra M. Z. Slawin, [ID] [a] Cristina Sissa, [ID] [b]
Francesco Azzolin,[b] Francesco Di Maiolo, [ID] [b] Anna Painelli [ID] *[b] and
Eli Zysman-Colman [ID] *[a]

We present the synthesis, optoelectronic characterization, and a detailed theoretical study of **DMAC-py-TRZ**, a novel, efficient TADF emitter. This compound is a structural relative of the well-known TADF compound **DMAC-TRZ**, substituting the bridging phenylene for a pyridyl group. This marginal change has an enormous impact on the structure and hence on the photophysics as the steric interactions between the DMAC donor and the bridge that force **DMAC-TRZ** into an orthogonal conformation are attenuated and permit **DMAC-py-TRZ** to adopt a planar and slightly bent structure in the ground state. The large degree of conjugation in the bent **DMAC-py-TRZ** structure, demonstrated by the strong intensity of the lowest excitation with CT character, is responsible for a large singlet triplet gap, hence hindering TADF of this bent conformer. The computational analysis predicts that emission occurs, however, from a relaxed orthogonal excited-state geometry, as confirmed by the huge Stokes shift observed in non-polar solvents. In this relaxed orthogonal geometry TADF is indeed observed. Emission from the unrelaxed state is recovered in glassy frozen solvents, where the emission band is largely blue-shifted compared with measurements in liquid solvent, and TADF is quenched. In amorphous matrices, structural disorder leads to the coexistence of both conformers, even if, depending on the emitter concentration, dual fluorescence may disappear due to a fast energy transfer from the bent to the orthogonal conformers. We maintain that this efficient energy transfer is responsible for the good efficiency of **DMAC-py-TRZ** devices, because of the presence in the matrix of a sizable proportion of compounds that adopt the bent structure, favorable to act as the host for the orthogonal TADF conformer of **DMAC-py-TRZ**.

10th Anniversary Statement

The *Journal of Materials Chemistry C* has been one of our favourite journals for OLED materials research. The quality and breadth of the science covered in the journal particularly in the area of emitter development for electroluminescent devices has been excellent. It is always a pleasure to peruse each week's table of contents and to then read exciting and new science in optoelectronic materials. We look forward to the next 10 years and beyond and will continue to support JMCC.

[a] *Organic Semiconductor Centre, EaStCHEM School of Chemistry, University of St Andrews, St Andrews, Fife, KY16 9ST, UK*
E-mail: eli.zysman-colman@st-andrews.ac.uk,
Web: https://www.zysman-colman.com; Tel: +44 (0)1334 463826
[b] *Department of Chemistry, Life Science and Environmental Sustainability, University of Parma, 43124 Parma, Italy*
† The research data supporting this publication can be accessed at **https://doi.org/10.17630/2152973b-5584-40ec-ac34-3f30c0d7893d**
‡ Electronic supplementary information (ESI) available. CCDC 2224273 and 2224274. For ESI and crystallographic data in CIF or other electronic format see DOI: **https://doi.org/10.1039/d2tc05213j**
§ Equal contribution.

Introduction

In an organic light-emitting diode (OLED), electrons and holes, injected in the device from opposite electrodes, combine to form excitons. According to spin statistics, 25% of the electrically generated excitons are in a singlet state and 75% are in a triplet state. If the excitons form on a fluorescent molecule, emission will only occur from the singlet excitons, effectively limiting the device Internal Quantum Efficiency (IQE). Phosphorescent dyes

harvest both singlet and triplet excitons to emit light from the triplet excited state resulting in an IQE of up to 100%. Most phosphorescent emitters, however, contain noble metals such as platinum or iridium, among the scarcest elements on Earth.[1–3] Thermally activated delayed fluorescence (TADF) offers a different yet equally appealing strategy to triplet harvesting where 100% IQE is also possible in the device. In TADF emitters, dark triplet excitons are thermally upconverted into emissive singlets *via* reverse intersystem crossing (RISC). RISC is possible when the energy gap, ΔE_{ST}, between the lowest lying singlet and triplet excited states is of the order of the thermal energy (*ca.* < 0.02 eV), provided that spin–orbit coupling (SOC) between the two states is non-negligible. To minimize ΔE_{ST}, the overlap between the HOMO and LUMO of the molecule must be reduced, localizing the two orbitals in separate electron-donating (for the HOMO) and electron-accepting (for the LUMO) parts of the molecule.[4] This separation is most often obtained by enforcing a large dihedral angle between the electron donor and acceptor moieties.[5] This strategy, however, leads to a reduction of the fluorescence efficiency and, according El Sayed rule,[6] to a reduction of the spin–orbit coupling between the singlet and triplet states as well.

Two of the most common moieties employed as donors and acceptors, respectively, are 9,9-dimethy-9,10-dihydroacridine (DMAC) and 2,4,6-triphenyl-1,3,5-triazine (TRZ), and the combination of the two produces the emitter DMAC-TRZ, first reported by Tsai *et al.*[7] **DMAC-TRZ** shows a very high photoluminescence quantum yield, Φ_{PL}, of 90%, at λ_{PL} of 495 nm, as an 8 wt% doped film in mCPCN [9-(3-(9H-carbazol-9-yl)phenyl)-9H-carbazole-3-carbonitrile]. In **DMAC-TRZ**, the ΔE_{ST} amounts

to a few tens of meV, depending on the host matrix, with a delayed fluorescence lifetime of 1.9 μs in mCBPBN, in line with an efficient RISC process.[8] The OLED shows a high maximum external quantum yield, EQE_{max}, of 26.5% at λ_{EL} of 500 nm, while devices prepared from neat DMAC-TRZ films show a comparable EQE_{max} of 20.0%.[7] The modest reduction of the EQE_{max} at high concentration can be understood in terms of the orthogonal conformation of the emitter, which effectively prevents aggregation. Both the doped and non-doped devices show a relatively small efficiency roll-off, with an EQE_{100} of 25.1% and 18.9%, respectively.

The emitters **a-DMAC-TRZ**[9] and **MA-TA**[10] are derivatives of DMAC-TRZ where adamantane groups are incorporated into the structure (Fig. 1). In **a-DMAC-TRZ**, the adamantane-functionalization of the donor moiety leads to a deformed structure that results in an increased optical gap and thus a bluer emission. Dual fluorescence is observed from two different conformers, but overall, the electroluminescence (EL) performance remains similar to the **DMAC-TRZ** OLED, with an EQE_{max} of 28.9%, yet with a λ_{EL} of 488 nm. In the report by Wada *et al.*,[10] the replacement of the distal phenyl moieties on the TRZ with adamantyl groups results in a weaker acceptor, leading to a blue-shifted electroluminescence compared to **DMAC-TRZ**. The adamantyl substitution also reduces the non-radiative decay leading to a Φ_{PL} of 99%. The blue solution-processed device (λ_{EL} of 475 nm) shows an EQE_{max} at 22.1%. Conversely, replacement of the distal phenyl rings in TRZ by electron-withdrawing pyrimidines (**DMAC-bPmT**) results in a red-shifted emission (λ_{PL} of 520 nm *vs.* 500 nm for **DMAC-TRZ** in toluene).[11] The delayed
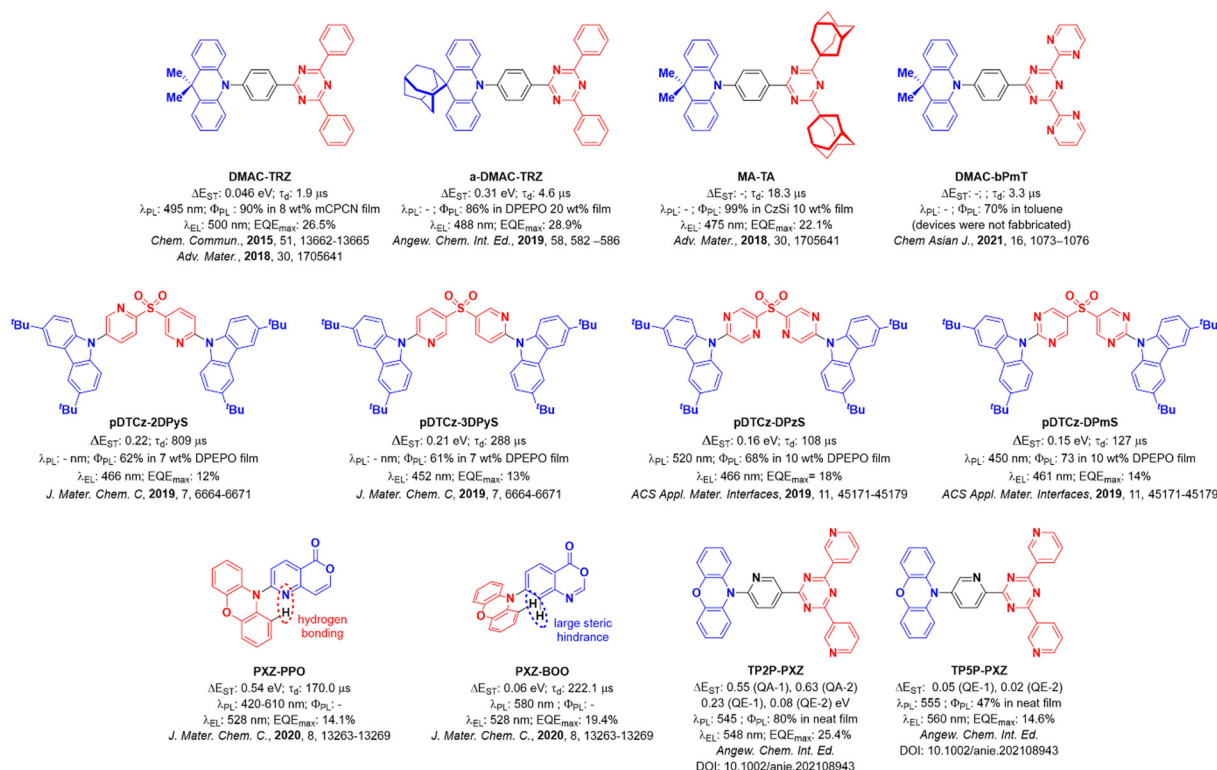

Fig. 1 Molecular structures of selected emitters from the literature with selected photophysical and device performance data.

This journal is © The Royal Society of Chemistry 2023

J. Mater. Chem. C, 2023, **11**, 8284–8292 | **8285**

emission lifetime of **DMAC-bPmT** is 3.3 μs in toluene, which is shorter than that of **DMAC-TRZ** at 8.8 μs in the same medium. The RISC rate constant, k_{RISC}, of **DMAC-bPmT** is 8.8×10^5 s^{-1}, is three times faster than that of **DMAC-TRZ** (2.9×10^5 s^{-1}). However, its Φ_{PL} of 70% in toluene is reduced compared to that of DMAC-TRZ (Φ_{PL} = 93% in toluene). Rajamalli et al.,[12] and Dos Santos et al.,[13] showed that the introduction of a heteroaromatic bridge in sulfone-based D–A TADF emitters can prevent structural relaxation, enhance Φ_{PL} and improve the color purity due to the narrower emission, and demonstrated an improvement in the efficiency of the devices compared to that with the reference emitter **pDTCz-DPS**. The materials in the study of Rajamalli et al.,[12] **pDTCz-2DPyS**, and **pDTCz-3DPyS**, both show good Φ_{PL} of ca. 60%. The blue OLEDs, at λ_{EL} of 466 nm and 452 nm for the devices with **pDTCz-2DPyS**, and **pDTCz-3Dpy**, respectively, showed EQE$_{max}$ ~12–13%, which are considerably improved over the parent device with **pDTCz-DPS** (EQE$_{max}$ of 4.7%). Dos Santos et al.,[13] showed that the addition of second nitrogen atom within the bridging heterocycle in **pDTCz-DPzS**, and **pDTCz-DPmS** contributed to a further enhancement of the EQE$_{max}$ to 18% and 14%, respectively, at λ_{EL} of 522 nm and 461 nm for the devices with **pDTCz-DPzS**, and **pDTCz-DPmS**, respectively.

The impact of intramolecular H-bonding on the photophysics of TADF emitters was also investigated by Chen et al. in two phenoxazine-based emitters **PXZ-PPO** and **PXZ-BOO**.[14] **PXZ-BOO** shows TADF, relevant devices having EQE$_{max}$ of 19.4% at λ_{EL} of 528 nm. In THF solution, **PXZ-PPO** is present as a mixture of two conformers, a more planar structure with N–H interaction and a twisted structure, where hydrogen bonding is not present. The planar conformation emits in the deep blue at 420 nm but shows no TADF, while the twisted conformer shows green TADF (610 nm) but with a very short lifetime of 170 ns. The planar conformer is dominant in the crystalline phase, while in solution the twisted conformer is largely responsible for the observed photophysics, giving rise to TADF. The **PXZ-PPO**-based device, with EQE$_{max}$ of 14.1% at λ_{EL} of 528 nm, is slightly inferior to the OLED based on **PXZ-BOO**, which has an EQE$_{max}$ of 19.4% at λ_{EL} of 528 nm.

The presence of two conformers of a TADF emitter has also been documented by Shi et al. in the TRZ derivative compounds **TP2P-PXZ** and **TP5P-PXZ**.[15] Phenoxazine and a central terpyridine bridge were used to promote the formation of an intramolecular hydrogen bond in **TP2P-PXZ**, while in the control compound **TP5P-PXZ** this interaction is absent. The presence of quasi-equatorial (QE) and quasi-axial (QA) conformations of **TP2P-PXZ** led to a self-doped system, where the QA conformer effectively acts as the host material. This led to an efficient OLED with an EQE$_{max}$ of 25.4% at λ_{EL} of 548 nm while the performance of the device with **TP5P-PXZ** was somewhat attenuated with an EQE$_{max}$ of 14.6% at a slightly red-shifted λ_{EL} of 560 nm. Similarly, two conformers have been found coexisting in the crystalline phase for the compounds **Trz-Py-NCS** and **Trz-Py-SAC**.[16]

These examples show that modification of the nature of the aromatic bridge in a TADF emitter can lead to significant changes in the molecular geometry, with the co-existence of different conformers that show distinctive photophysics. In this
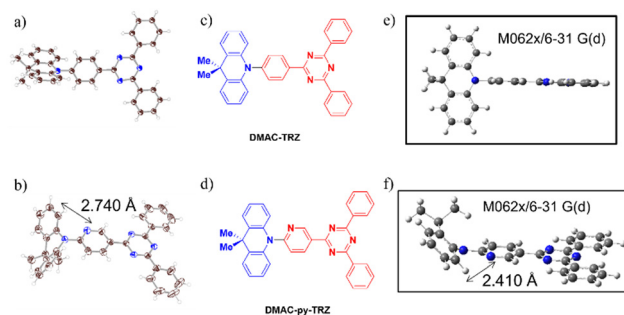

Fig. 2 (a) and (b) The crystal structure shown as ORTEP at 50% ellipsoid probability; (c) and (d) the molecular structure; (e) and (f) the calculated ground state structure of **DMAC-TRZ** and **DMAC-py-TRZ**.

work, we introduce the emitter **DMAC-py-TRZ**, where the phenylene bridge in **DMAC-TRZ**[7] is replaced by a 2-pyridyl bridge. **DMAC-py-TRZ** emits at λ_{PL} of 539 nm and has a Φ_{PL} of 58% in toluene solution while as a 10 wt% doped mCP film the Φ_{PL} is 496 nm and the Φ_{PL} is 57%. Its crystal structure (Fig. 2) documents a small dihedral angle between the DMAC and pyridyl bridge of 19.7(2)° and a V-shaped or bent structure of the DMAC donor, with an associated bending angle (deviation from a planar conformation) of 45°. This behaviour is in line with that observed by Shi et al.[15] We present an in-depth computational study and an extensive optoelectronic and photophysical characterization that showcases the impact that conformational changes in the excited state and not just in the ground state have on the photophysics of the compound.

Results and discussion

Computational analysis

The ground-state geometries of **DMAC-TRZ** and **DMAC-py-TRZ** were optimized in the gas phase using density functional theory (DFT) at the M062X/6-31G(d) level of theory.[17–19] The excited-state energies were calculated using time-dependent density functional theory (TD-DFT) within the Tamm–Dancoff approximation[20] at the same level of theory (TDA-DFT). We employ the term "orthogonal" to describe the structure with a dihedral angle between the DMAC and the bridge that is close to 90° and we dub as "bent" the structure with the small dihedral angle and V-shaped geometry of the DMAC.

In a recent publication,[21] an extensive computational analysis of DMAC-TRZ set the basis for a few-state model that was carefully validated against spectroscopic properties in solution. Then the same model was exploited to calculate ISC and RISC rate constants, also accounting for environmental effects including dielectric and conformational disorder.[22,23] In the ground-state equilibrium geometry of **DMAC-TRZ**, the DMAC and TRZ moieties are mutually orthogonal (Fig. 2), in line with the crystal structure.[21] In this orthogonal geometry, the S$_1$ and T$_1$ states each have a pure charge transfer (CT) character. In other terms, the HOMO and LUMO have negligible overlap so that the singlet–triplet gap is almost closed, with ΔE_{ST} = 0.01 eV. The close similarity between the orbitals involved in S$_1$ and T$_1$ states

8286 | J. Mater. Chem. C, 2023, **11**, 8284–8292

This journal is © The Royal Society of Chemistry 2023

implies a vanishing SOC, according to El Sayed's rule,[6] as to hinder direct RISC from T_1 to S_1.

As for the excited states of **DMAC-TRZ**, S_1 (with a strong ^{1}CT character) retains an orthogonal geometry, while T_1 (^{3}CT) undergoes a large conformational deformation where the dihedral becomes ~60°. At this angle, ΔE_{ST} increases as does SOC. A rigid scan of the dihedral angle of DMAC-TRZ (Fig. S9c, ESI‡)[21] is informative. Specifically, starting from the optimized ground-state geometry, we calculated the ground and excited state energies upon gradual rotation of the DMAC unit about the phenylene bridge without allowing for any additional molecular relaxation (the dihedral angle for the scan is defined in Fig. S9a, ESI‡). The resulting S_0, S_1, T_2 and T_3 potential energy surfaces (PES) all show a flat minimum for the orthogonal geometry, while T_1 shows a double minimum around $(90 \pm 30)°$ angle.[19] The molecular orbitals (MOs) and natural transition orbitals (NTOs) shown in Fig. S11 and S12 (ESI‡) reveal that in the orthogonal structure, the HOMO is localized on DMAC and the LUMO is on the TRZ.

In contrast with **DMAC-TRZ**, the ground-state optimized geometry of **DMAC-py-TRZ** has a bent structure (Fig. 2f), as also observed in the crystal structure (Fig. 2b). To better understand the structural differences between **DMAC-TRZ** and **DMAC-py-TRZ**, a rigid dihedral angle scan of **DMAC-py-TRZ** starting from an analogous orthogonal conformation to that of **DMAC-TRZ** has been performed. The rigid scan leads to a qualitatively similar picture for the two compounds (Fig. S9, ESI‡), with relevant MOs and NTOs in Fig. S11 and S12 (ESI‡), showing the HOMO and LUMO localized on the donor and acceptor moieties, respectively. The presence of the nitrogen atom in the pyridine bridge effectively increases the electron-withdrawing strength of the acceptor, resulting in a stabilized LUMO and a smaller HOMO–LUMO gap in **DMAC-py-TRZ** ($E_{HOMO-LUMO}$ = 4.78 eV for the orthogonal structure) *vs.* **DMAC-TRZ** ($E_{HOMO-LUMO}$ = 4.99 eV for the orthogonal structure). Accordingly, the S_1 and T_1 excitations occur at lower energy in **DMAC-py-TRZ** than in **DMAC-TRZ** and both the S_1 and T_1 states are stabilized compared to those of **DMAC-TRZ** (Fig. S9c and d, ESI‡). The rigid energy scan, however, points to a large increase of the ground-state energy when the dihedral angle deviates significantly from orthogonality, so that non-orthogonal conformations are hardly accessible. To address the bent conformer, we performed a relaxed scan of the dihedral angle, relevant results being shown in Fig. 3 (see also ESI,‡ Fig. S18).

The relaxed scans show that for each of the emitters, two minima are present, corresponding to the orthogonal and bent structures. For **DMAC-TRZ**, the energy difference between the two conformers amounts to 0.04 eV, slightly larger than thermal energy at room temperature. The energy barrier for the interconversion between the two conformers, 0.22 eV (21.2 kcal mol^{-1}), is, however, much larger than thermal energy so that only the orthogonal geometry is expected to be significantly populated at room temperature. The situation is very different for **DMAC-py-TRZ** where the bent conformer (dihedral angle ~10°) is lower in energy than the orthogonal conformer by 0.20 eV and the energy barrier for the interconversion between the bent and orthogonal
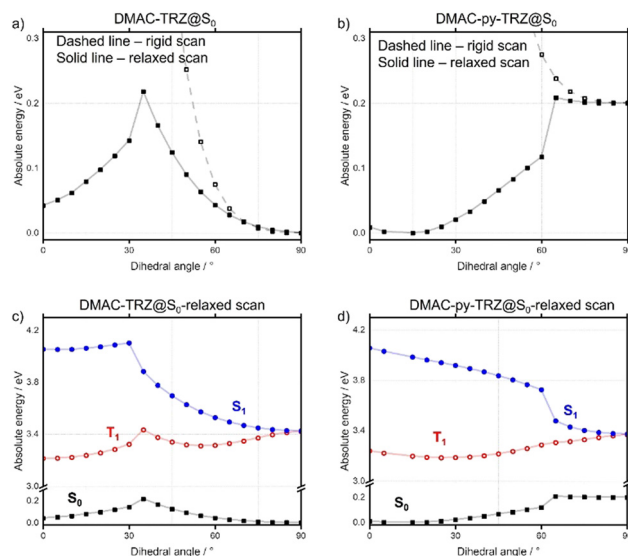

Fig. 3 (a) and (b) compare the ground state (S_0) energy calculated as a function of the dihedral angle in a rigid (dashed lines) and relaxed scan (continuous lines) for **DMAC-TRZ** and **DMAC-py-TRZ**, respectively; (c) and (d) show the energies of the S_0, S_1 and T_1.

conformers is 0.20 eV (19.3 kcal mol^{-1}). Thus, at room temperature only the bent conformer is populated. The MOs and NTOs calculated for the bent structure (Fig. S11 and S12, ESI‡) show that in both molecules there is a partial delocalization of the HOMO onto the acceptor moiety and, for **DMAC-py-TRZ** also a partial delocalization of the LUMO onto the donor moiety.

Divergent results are obtained for the excited state energies at the geometries relevant to the rigid/relaxed scans of the dihedral angle (Fig. 3c and d) of the two compounds. For **DMAC-TRZ**, the rigid (Fig. S9c, ESI‡) and the relaxed scans (Fig. 3c) lead to the same picture: the S_1 state maintains the same orthogonal conformation as the ground state, while the T_1 state is stabilized and adopts a twisted structure (dihedral angle: ~60°). Full optimisations of S_1 and T_1 confirm this result.[21] In the orthogonal geometry, the S_1 state is an almost pure CT state and, hence, has a negligible oscillator strength. The scenario is much more interesting for **DMAC-py-TRZ**. In the bent geometry (the energy minimum, Fig. 3b), the vertical excitation energy to S_1 amounts to 4.034 eV and the ΔE_{ST} is 0.786 eV, which is far too large for TADF to be operational at ambient temperature. Moreover, the oscillator strength for the $S_0 \rightarrow S_1$ is large (1.27, Fig. S12c, ESI‡) in this geometry due to the significant overlap of the orbitals involved in the transition (Fig. 4a). However, the bent geometry is not the equilibrium geometry for S_1 (Fig. 4d) and a huge structural deformation is predicted in the S_1 state from the bent to the orthogonal structure. In other terms, in **DMAC-py-TRZ** the absorption occurs from the bent geometry and the lowest energy transition is both high in energy and has a large oscillator strength. By contrast, fluorescence occurs from the orthogonal structure at a much lower energy (3.17 eV) and with negligible oscillator strength (as per the non-overlapping orbitals, in Fig. 4b). In this orthogonal geometry the ΔE_{ST} reduces to only 8.2 meV), making TADF possible. To better appreciate the
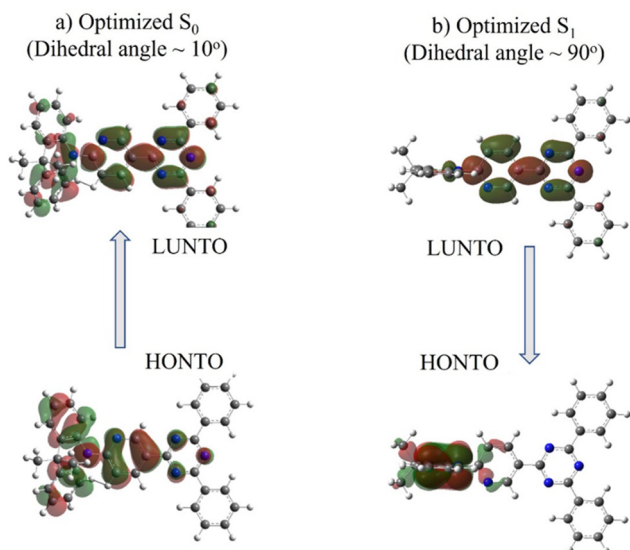
Fig. 4 NTOs of **DMAC-py-TRZ** calculated for the S_0-S_1 transition (a) at the S_0-optimized geometry, which is relevant to the absorption process; (b) at the S_1-optimized geometry, which is relevant to the emission process.

differing photophysics of the two different conformers in either **DMAC-TRZ** or **DMAC-py-TRZ**, Fig. S19 (ESI‡) compares relevant calculated spectra and Table S29 (ESI‡) summarizes the calculated ΔE_{ST}.

In **DMAC-py-TRZ**, the T_1 state is predicted to exist as a twisted geometry in both the rigid (Fig. S9d, ESI‡) and relaxed scans (Fig. 3d). The full optimization of the excited state geometry, however, yields conflicting results. For S_1 the situation is clear: taking either the bent or the orthogonal geometry as starting points for the excited state optimization, the S_1 geometry (Fig. 3d) always converges to the orthogonal conformation, supporting the results from the relaxed scan analysis. For T_1, instead, two different structures are reached depending on the starting geometry (Fig. S10, ESI‡), with slightly different $\Delta E_{S_1-T_1}$ values (0.93 eV where the dihedral angle is 30° and 0.41 eV where the dihedral angle is 60°). The energy of the two triplet conformations is similar ($\Delta E_{T_1\ 60°-30°} = 0.07$ eV), so that a firm conclusion about the equilibrium geometry for T_1 cannot be reached.

Optoelectronic properties

Cyclic Voltammetry (CV) and Differential Pulse Voltammetry (DPV) of **DMAC-py-TRZ** and **DMAC-TRZ** were measured in degassed DCM with tetra-*n*-butylammonium hexafluorophosphate as the electrolyte and Fc/Fc$^+$ as the internal reference. The voltammograms in Fig. 5a are reported *versus* a Saturated Calomel Electrode (SCE). Both materials show pseudo-reversible reduction and oxidation waves. Both oxidation and reduction waves for **DMAC-py-TRZ** ($E_{ox}/E_{red} = 1.11/-1.64$ V) are anodically shifted compared to those of **DMAC-TRZ** (0.97/−1.72 V). The corresponding HOMO and LUMO energies are −5.31/−2.62 eV and −5.45 eV/−2.70 eV for **DMAC-TRZ** and **DMAC-py-TRZ**, respectively. Comparing electrochemical redox gaps measured in solution with gas-phase DFT results is tricky.[25,26] Experimentally, the
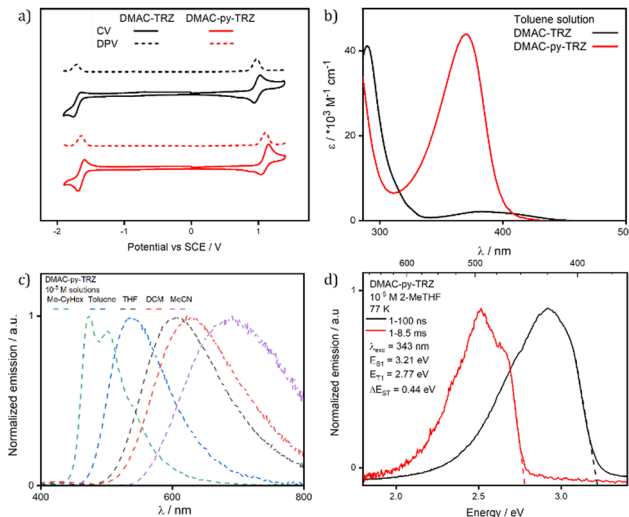

Fig. 5 (a) Cyclic voltammetry (CV) and differential pulse voltammetry (DPV) of DMAC-TRZ (black) and DMAC-py-TRZ (red) in DCM (scan rate = 100 mV s^{-1}, tetrabutylammonium hexafluorophosphate as electrolyte, reported relative to a saturated calomel electrode (SCE) with a ferrocene/ferrocenium (Fc/Fc$^+$) redox couple as the internal standard, 0.46 V *vs.* SCE for DCM[24]). (b) UV-vis absorption spectra of **DMAC-TRZ** (black) and **DMAC-py-TRZ** (red) in 10^{-5} M toluene. (c) Solvatochromism photoluminescence study of **DMAC-py-TRZ** ($\lambda_{exc,}$ = 340 nm); (d) prompt fluorescence and phosphorescence spectra at 77 K in 10^{-5} M 2-methyltetrahydrofuran (2-MeTHF) glass (λ_{exc} = 343 nm, prompt and delayed fluorescence spectra were obtained in the 1–100 ns and 1–8.5 ms time range, respectively).

HOMO–LUMO gap of **DMAC-py-TRZ**, ∼2.75 eV, is larger than the HOMO–LUMO gap of **DMAC-TRZ** ∼2.69 eV. Considering an orthogonal geometry for both dyes, DFT results for the HOMO–LUMO gaps are 4.78 eV and 4.99 eV for **DMAC-py-TRZ** and **DMAC-TRZ**, respectively, showing the opposite trend *vs.* experiment. The same is true if the bent geometry is considered for both dyes, with calculated HOMO–LUMO gaps of 5.73 eV and 5.77 eV for **DMAC-py-TRZ** and **DMAC-TRZ**, respectively. However, if we properly consider an orthogonal structure for **DMAC-TRZ** ($E_{HOMO-LUMO} = 4.99$ eV for orthogonal geometry) and a bent structure for **DMAC-py-TRZ** ($E_{HOMO-LUMO} = 5.73$ eV for bent geometry), calculated HOMO–LUMO gaps reflect the trend observed experimentally. A better estimate of the ionization potential (IP) and electron affinity (EA) of both dyes is obtained by comparing the energy of the radical cation and radical anion molecules in their relaxed geometry with the energy of the neutral dye: IP = $E_{radical\ cation} - E_{neutral}$ and EA = $E_{radical\ anion} - E_{neutral}$. In this case, the IP-EA gap (to be compared with the experimental data) are 7.59 eV and 7.24 eV for **DMAC-py-TRZ** and **DMAC-TRZ**, respectively, for the orthogonal geometries. For the bent geometries, the gaps are 7.63 eV and 7.25 eV for **DMAC-py-TRZ** and **DMAC-TRZ**, respectively. Also in this case, if we consider the orthogonal conformer for **DMAC-TRZ** and a bent conformer for **DMAC-py-TRZ** the calculated gaps reflect the trend observed experimentally. A perfect agreement between DFT estimates and experimental data is, however, not expected since our gas-phase calculations do not account for solvation effects.[25,26] In any case, the HOMO stabilization in **DMAC-py-TRZ** *vs.* **DMAC-TRZ** is ascribed to the presence of the electron-withdrawing pyridyl

8288 | *J. Mater. Chem. C*, 2023, **11**, 8284–8292

This journal is © The Royal Society of Chemistry 2023

bridge, which reduces the electron density on the donor. Similarly, the electron density of the acceptor is reduced, resulting in a more stabilized LUMO level.

Fig. 5b compares the absorption spectra of **DMAC-TRZ** and **DMAC-py-TRZ** in toluene. The CT band of **DMAC-py-TRZ** at 370 nm is slightly blue-shifted with respect to **DMAC-TRZ** at 382 nm. The most striking difference is recognized, however, in the much larger intensity of the band measured for **DMAC-py-TRZ** (ε = 43 800 M^{-1} cm^{-1}) *vs.* **DMAC-TRZ** (ε = 2100 M^{-1} cm^{-1}). This is a direct consequence of the different conformations adopted by the two compounds in the ground state: the orthogonal conformation of **DMAC-TRZ** (observed in the crystal structure and predicted by DFT) hinders an effective conjugation and suppresses the intensity of the low-energy CT transition. On the other hand, the bent conformation of **DMAC-py-TRZ** (observed in the crystal structure and predicted by DFT) promotes an efficient conjugation of the two moieties, perfectly in line with the oscillator strength calculated with TD-DFT (oscillator strengths are reported in Fig. S12 (ESI‡), together with NTOs).

Neither the absorption spectra of **DMAC-TRZ** and **DMAC-py-TRZ** (Table S27, ESI‡) show solvatochromism, in line with a very small permanent dipole moment of the molecule in the ground state. Photoluminescence (PL) spectra or **DMAC-py-TRZ** in Fig. 5c (Table S27, ESI‡) show a strong positive solvatochromism akin to that observed for **DMAC-TRZ** (Fig. S13 and ref. 20, ESI‡) The large positive PL solvatochromism observed for both compounds suggests that the emissive excited state has a large permanent dipole moment, thus confirming the CT character of this state in both compounds.[27,28] The progressive broadening of the emission band in the solvatochromism study is a result of polarity-induced inhomogeneous broadening.[28,29] The well-resolved vibronic structure of the emission band in non-polar solvents is often considered an indication of a local nature of the relevant excitation. Therefore, to prove the CT nature of the lowest transition in **DMAC-py-TRZ** in all solvent, including non-polar ones, Fig. S14 (ESI‡) shows spectra collected for the two molecular fragments, **DMAC** and **py-TRZ**. For **py-TRZ**, only absorption spectra are shown since the species is not emissive. The spectroscopic features of both molecular fragments are located at higher energies than the lowest energy feature seen in **DMAC-py-TRZ**, confirming that this specific feature is related to a CT state. An important and unusual result is recognized in the large Stokes shift observed for **DMAC-py-TRZ** in non-polar solvents (Table S27, ESI‡): in methylcyclohexane, the absorption band is located at 370 nm, while the emission is seen at 472 nm, amounting to a Stokes shift of ∼0.7 eV. This large Stokes shift can only be explained in terms of a very large molecular relaxation upon photoexcitation, well in line with the TD-DFT results that predict the relaxation of the S_1 state from the bent to the orthogonal geometry.

In degassed toluene, **DMAC-TRZ** and **DMAC-py-TRZ** have similar Φ_{PL} of 67% and 58%, respectively, in line with emission originating in both compounds from a similar orthogonal geometry. The Φ_{PL} decrease in air (Φ_{PL} = 22% and 17%, respectively), indicating the presence of accessible triplet excited states. The prompt and delayed lifetimes, τ_p and τ_d, for **DMAC-TRZ** in degassed toluene are of 20.8 ns (1.1%) and 5.2 μs (98.9%), in line with those previously reported,[7] while the τ_p and τ_d for **DMAC-py-TRZ** are 44.0 ns (8.1%) and 1.5 μs (91.9%), respectively (Fig. S15, ESI‡).

To summarize, theoretical and spectroscopic studies agree with the picture where **DMAC-TRZ** maintains the same orthogonal conformation in both the ground and the S_1 states. However, **DMAC-py-TRZ** undergoes a significant geometric reorganization from the bent geometry in the ground state to the orthogonal geometry in the excited state.

Spectra collected in a glassy 2-MeTHF matrix at 77 K (Fig. 5d) shed further light on the geometrical relaxation of **DMAC-py-TRZ** upon photoexcitation. In the frozen matrix, the emission peaks at 404 nm, blue-shifted compared to that in liquid 2-MeTHF at ambient conditions (λ_{PL} = 596 nm, Table 1 and Fig. S16, ESI‡). Apparently, in the frozen matrix the excited compound cannot relax, so that emission occurs from the bent structure and hence peaks at much higher energy than in the (non-polar) liquid solvent. The gated signal collected in the glassy matrix (red line in Fig. 5d) is ascribed to phosphorescence, suggesting a large ΔE_{ST} for this conformer under these conditions, again in line with that calculated for the bent structure.

The PL behavior of **DMAC-py-TRZ** was also characterized in polyTHF, a viscous solvent where conformational relaxation is hindered. Interestingly, two emission bands are observed in this viscous medium (Fig. S17, ESI‡). The first emission band at

Table 1 Photophysical properties of **DMAC-TRZ** and **DMAC-py-TRZ** (*cf.* Table S28, ESI)

Material	Environment	$\lambda_{PL}{}^a$/nm	Φ_{PL} N$_2$ (air)^b/%	τ_p, $\tau_d{}^e$; ns; μs	$S_1{}^f$/eV	$T_1{}^g$/eV	$\Delta E_{ST}{}^h$/eV
DMAC-TRZ	Toluene (10^{-5} M)[31]	499	67 (22)^c	20.8; 5.2	2.88	2.57	0.31
	mCP 10 wt%	499	47 (45)	22.9; 15.3	—	—	—
	PMMA 10 wt%	523	18 (15)	41.6; 17.0	—	—	—
DMAC-py-TRZ	Toluene (10^{-5} M)	539	58 (17)^c	44.0; 1.5	3.21	2.77	0.44
	mCP 10 wt%	496	57 (54)^d	24.9; 5.3	—	—	—
	PMMA 10 wt%	516	64 (58)^d	26.0; 4.7	—	—	—

^{a} Measured at room temperature. ^{b} λ_{exc} = 340 nm. ^{c} Obtained *via* the optically dilute method[32] (see ESI), quinine sulfate (0.5 M) in H_2SO_4 (aq) was used as the reference, Φ_{PL}: 54.6%, λ_{exc} = 360 nm.[33] ^{d} Obtained using an integrating sphere. ^{e} τ_p (prompt lifetime) and τ_d (delayed lifetime) were obtained from the transient PL decay of degassed solution/doped film, λ_{exc} = 378 nm. ^{f} S_1 was obtained from the onset of the prompt fluorescence measured at 77 K, obtained in the 1–100 ns time range. ^{g} T_1 was obtained from the onset of the phosphorescence spectrum measured at 77 K, obtained in the 1–8.5 ms time range. ^{h} ΔE_{ST} = S_1 − T_1.

This journal is © The Royal Society of Chemistry 2023

J. Mater. Chem. C, 2023, **11**, 8284–8292 | **8289**

410 nm is similar to the one observed in the glassy matrix at 77 K while the second emission at 600 nm is similar to the emission observed in DMSO at room temperature. At ambient temperature, the excited state relaxation, fully hindered in glassy matrices at low temperature, is only partially hindered in the viscous polyTHF. Accordingly, the presence of the two emission bands is evidence of the simultaneous presence of the unrelaxed (bent) emissive species (as in the glassy matrix) as well as of relaxed (orthogonal) species (as in the liquid solvent).

Having observed that the S_1 relaxation of **DMAC-py-TRZ** in frozen glassy matrices at low temperature is fully hindered while it is only partially hindered in viscous solvents at ambient condition, we next transitioned to an investigation of the behavior of this compound in amorphous matrices where large geometric reorganization is also likely to be hindered (Fig. 6). Spin-coated thin films of **DMAC-py-TRZ** doped into PMMA at 10 wt% were first prepared (Fig. 6a). Emission at λ_{PL} of 516 nm was observed with a Φ_{PL} of 63.8% under a N_2 atmosphere, which decreased to 58.0% upon exposure to oxygen. Biexponential decay kinetics were observed in the time-resolved PL measurements, with τ_p of 26.0 ns and an average τ_d of 4.7 μs [$\tau_1 = 1.0$ μs (32.6%), $\tau_2 = 7.4$ μs (67.4%)], respectively. The presence of a delayed fluorescence suggests that at least some emitter molecules adopt an orthogonal conformation, as to allow for TADF. Compared to the data obtained in toluene (τ_p of 44.0 ns and τ_d of 1.5 μs), **DMAC-py-TRZ** possesses a shorter-lived prompt component and a slightly longer-lived delayed component. We then investigated the photophysics in mCP (1,3-bis(N-carbazolyl)benzene) as the host matrix, a suitable high triplet energy host for both compounds that would be relevant for OLEDs. Fig. 6d shows results at a 10 wt% doping
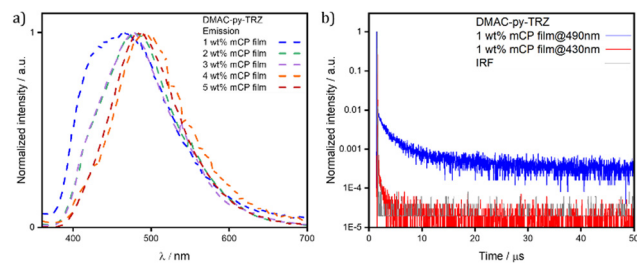

Fig. 7 (a) Emission spectra of **DMAC-py-TRZ** in spin-coated 1–5 wt% mCP films (λ_{exc} = 340 nm); (b) time-resolved PL decay in spin-coated 1 wt% mCP film of **DMAC-py-TRZ** collected at λ_{em} = 490 nm and λ_{em} = 430 nm (λ_{exc} = 378 nm).

concentration. The emission in mCP is blue-shifted at τ_{PL} of 496 nm, compared to that of the doped PMMA film. The Φ_{PL} of the doped film in mCP is 57.4% under N_2, which decreased to 53.5% in air. The τ_p = 24.9 ns and the average τ_d = 5.3 μs [$\tau_1 = 1.4$ μs (46.8%), $\tau_2 = 7.7$ μs (53.2%)]. In both PMMA and mCP matrices at 10% doping the delayed emission is thermally activated (Fig. 7). However, extracting detailed information from such highly doped matrices is dangerous because of spurious phenomena, including homo energy-transfer and inner filter effects (self-absorption). Specifically, the ΔE_{ST} could be largely underestimated in films at 10% dye concentration due to self-absorption that moves the apparent onset of the absorption peak to the red. However, extracting the ΔE_{ST} from rates is similarly dangerous in view of the large error bars associated with rates.[30]

To minimize spurious concentration effects, low-concentration (down to 1 wt%) films were fabricated, relevant spectra being shown in Fig. 7. In these films both the high frequency emission originating from the bent structure, and the low-frequency emission from the orthogonal structure, are present, suggesting that both conformers are present in all films. The high frequency emission decays much more rapidly (Fig. 7b), again confirming that it originates from the bent conformer. Upon increasing concentration, the high frequency emission progressively weakens and disappears for doping concentrations above 3 wt%.

Two phenomena may exist to explain this observation, both related to the large transition dipole moment (large oscillator strength) of the $S_0 \rightarrow S_1$ transition in the bent geometry: (1) self-absorption; and (2) energy transfer from the bent to the orthogonal structure. Both phenomena are expected to become more efficient upon increasing the concentration of the emitter in the host matrix.

Fig. 6 (a) PL spectra of **DMAC-py-TRZ** in spin-coated 10 wt% mCP film, spin-coated 10 wt% PMMA film (λ_{exc} = 340 nm); (b) time-resolved PL decay in spin-coated 10 wt% mCP film of **DMAC-py-TRZ** (λ_{exc} = 378 nm); (c) temperature-dependent delayed fluorescence decays in spin-coated 10 wt% mCP film of **DMAC-py-TRZ** (λ_{exc} = 378 nm); (d) prompt fluorescence and phosphorescence spectra at 77 K in drop-cast 10 wt% mCP film (λ_{exc} = 343 nm, prompt and delayed fluorescence spectra were obtained in the 1–100 ns and 1–8.5 ms time range, respectively).

Conclusions

The synthesis of a new TADF emitter, **DMAC-py-TRZ**, is presented, together with an extensive computational analysis and experimental characterization. The chemical structure of **DMAC-py-TRZ** only marginally differs from that of the parent **DMAC-TRZ** compound. However, this minor change of the bridging moiety between the donor and acceptor has an
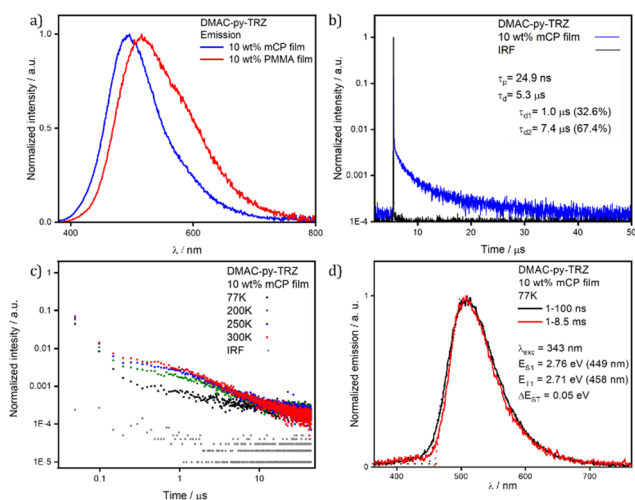
8290 | J. Mater. Chem. C, 2023, **11**, 8284–8292

This journal is © The Royal Society of Chemistry 2023

enormous impact on the conformation and hence on the photophysics of the compound. Specifically, while **DMAC-TRZ** maintains the same orthogonal geometry in both the ground and the first excited singlet states, **DMAC-py-TRZ** assumes a bent geometry in the ground state, as highlighted by the large oscillator strength measured in solution for this dye. However, upon excitation to the S_1 state, the system undergoes a large geometrical rearrangement to the orthogonal structure. This large relaxation is confirmed by the very large Stokes shift measured in non-polar solvents. In frozen 2-MeTHF glass at very dilute conditions, the relaxation is hindered and only a blue-shifted emission is seen from the unrelaxed bent conformer, without any hint of emission from the orthogonal structure. In mCP films a distribution of conformers exists and at low concentrations dual emission is observed, originating both from both the bent and orthogonal structures. However, upon increasing the doping concentration, the emission from the orthogonal conformer dominates. While self-absorption can be partly responsible for the phenomenon, we conclude that an efficient energy transfer from one conformer to the other also contributes to the spectral change. Indeed, TADF is not expected nor observed in the bent structure, due to a too large ΔE_{ST}. The good TADF efficiency of **DMAC-py-TRZ** in solution, similar as for **DMAC-TRZ**, is in line with the very fast molecular relaxation from the bent (TADF-silent) to the orthogonal geometry (TADF-active) in solution. The situation is more delicate in matrices where the host rigidity hinders a large molecular rearrangement. The observed good efficiency of TADF in matrices then suggests efficient energy transfer of excitons created on the bent (and TADF silent) structures towards molecules in the orthogonal (and TADF-active) structure as to retrieve all photogenerated singlet states for TADF activity. Most probably, efficient triplet-to-triplet energy transfer is also required to explain the good efficiency of **DMAC-py-TRZ** OLEDs, but this will be subject of a subsequent study.

Conflicts of interest

There are no conflicts to declare.

Note added after first publication

This article replaces the version published on 5 April 2023, in which Table 1 included values of S_1 and T_1 (as well as their difference, ΔE_{ST}) for the environments mCP 10 wt% and PMMA 10 wt%, for each of the materials **DMAC-TRZ** and **DMAC-py-TRZ**. These values have been removed in the current version because the authors no longer believe they can accurately measure them due to self-absorption, as is explained in the article. For completeness, the removed values of S_1 and T_1 have instead been included in the ESI,‡ where they can be found in Table S28.

Acknowledgements

Notes and references

1 C. Adachi, *Jpn. J. Appl. Phys.*, 2014, **53**, 060101.
2 M. Y. Wong and E. Zysman-Colman, *Adv. Mater.*, 2017, **29**, 1605444.
3 F. M. Xie, J. X. Zhou, Y. Q. Li and J. X. Tang, *J. Mater. Chem. C*, 2020, **8**, 9476–9494.
4 F. B. Dias, T. J. Penfold and A. P. Monkman, *Methods Appl. Fluoresc.*, 2017, **5**, 012001.
5 B. Milián-Medina and J. Gierschner, *Org. Electron.*, 2012, **13**, 985–991.
6 M. A. El-Sayed, *J. Chem. Phys.*, 1963, **38**, 2834–2838.
7 W. L. Tsai, M. H. Huang, W. K. Lee, Y. J. Hsu, K. C. Pan, Y. H. Huang, H. C. Ting, M. Sarma, Y. Y. Ho, H. C. Hu, C. C. Chen, M. T. Lee, K. T. Wong and C. C. Wu, *Chem. Commun.*, 2015, **51**, 13662–13665.
8 K. Stavrou, L. G. Franca and A. P. Monkman, *ACS Appl. Electron. Mater.*, 2020, **2**, 2868–2881.
9 W. Li, X. Cai, B. Li, L. Gan, Y. He, K. Liu, D. Chen, Y. C. Wu and S. J. Su, *Angew. Chem., Int. Ed.*, 2019, **58**, 582–586.
10 Y. Wada, S. Kubo and H. Kaji, *Adv. Mater.*, 2018, **30**, 1705641.
11 Y. Wada, H. Nakagawa and H. Kaji, *Chem. – Asian J.*, 2021, **16**, 1073–1076.
12 P. Rajamalli, D. Chen, W. Li, I. D. W. Samuel, D. B. Cordes, A. M. Z. Slawin and E. Zysman-Colman, *J. Mater. Chem. C*, 2019, **7**, 6664–6671.
13 P. L. Dos Santos, D. Chen, P. Rajamalli, T. Matulaitis, D. B. Cordes, A. M. Z. Slawin, D. Jacquemin, E. Zysman-Colman and I. D. W. Samuel, *ACS Appl. Mater. Interfaces*, 2019, **11**, 45171–45179.
14 J. X. Chen, Y. F. Xiao, K. Wang, X. C. Fan, C. Cao, W. C. Chen, X. Zhang, Y. Z. Shi, J. Yu, F. X. Geng, X. H. Zhang and C. S. Lee, *J. Mater. Chem. C*, 2020, **8**, 13263–13269.
15 Y. Shi, K. Wang, S. Zhang, X. Fan, Y. Tsuchiya, Y. Lee, G. Dai, J. Chen, C. Zheng, S. Xiong, X. Ou, J. Yu, J. Jie, C. Lee, C. Adachi and X. Zhang, *Angew. Chem.*, 2021, **133**, 26082–26087.
16 X. Fan, K. Wang, Y. Shi, D. Sun, J. Chen, F. Huang, H. Wang, J. Yu, C. Lee and X. Zhang, *SmartMat*, 2023, **4**, e1122.
17 Y. Zhao and D. G. Truhlar, *Theor. Chem. Acc.*, 2008, **120**, 215–241.
18 G. A. Petersson, A. Bennett, T. G. Tensfeldt, M. A. Al-Laham, W. A. Shirley and J. Mantzaris, *J. Chem. Phys.*, 1988, **89**, 2193–2218.

This journal is © The Royal Society of Chemistry 2023

J. Mater. Chem. C, 2023, **11**, 8284–8292 | **8291**

19 G. A. Petersson and M. A. Al-Laham, *J. Chem. Phys.*, 1988, **94**, 6081–6090.

20 S. Hirata and M. Head-Gordon, *Chem. Phys. Lett.*, 1999, **314**, 291–299.

21 R. Dhali, D. K. A. Phan Huu, F. Bertocchi, C. Sissa, F. Terenziani and A. Painelli, *Phys. Chem. Chem. Phys.*, 2021, **23**, 378–387.

22 D. K. A. Phan Huu, S. Saseendran and A. Painelli, *J. Mater. Chem. C*, 2022, **10**, 4620–4628.

23 D. K. A. Phan Huu, S. Saseendran, R. Dhali, L. G. Franca, K. Stavrou, A. Monkman and A. Painelli, *J. Am. Chem. Soc.*, 2022, **144**, 15211–15222.

24 W. E. Connelly and N. G. Geiger, *Chem. Rev.*, 1996, **96**, 877–910.

25 R. Dhali, D. K. A. Phan Huu, F. Terenziani, C. Sissa and A. Painelli, *J. Chem. Phys.*, 2021, **154**, 134112–134119.

26 D. K. A. Phan Huu, R. Dhali, C. Pieroni, F. Di Maiolo, C. Sissa, F. Terenziani and A. Painelli, *Phys. Rev. Lett.*, 2020, **124**, 107401.

27 A. Painelli and F. Terenziani, *Chem. Phys. Lett.*, 1999, **312**, 211–220.

28 B. Boldrini, E. Cavalli, A. Painelli and F. Terenziani, *J. Phys. Chem. A*, 2002, **106**, 6286–6294.

29 F. Terenziani, A. Painelli, A. Girlando and R. M. Metzger, *J. Phys. Chem. B*, 2004, **108**, 10743–10750.

30 M. Zheng, Y. Li, Y. Wei, L. Chen, X. Zhou and S. Liu, *J. Phys. Chem. Lett.*, 2022, **13**, 2507–2515.

31 Z. Zhang, E. Crovini, P. L. dos Santos, B. A. Naqvi, D. B. Cordes, A. M. Z. Slawin, P. Sahay, W. Brütting, I. D. W. Samuel, S. Bräse and E. Zysman-Colman, *Adv. Opt. Mater.*, 2020, **8**, 2001354.

32 G. A. Crosby and J. N. Demas, *J. Phys. Chem.*, 1971, **75**, 991–1024.

33 F. Song, Z. Xu, Q. Zhang, Z. Zhao, H. Zhang, W. Zhao, Z. Qiu, C. Qi, H. Zhang, H. H. Y. Sung, I. D. Williams, J. W. Y. Lam, Z. Zhao, A. Qin, D. Ma and B. Z. Tang, *Adv. Funct. Mater.*, 2018, **28**, 1800051.